

Article

Mapping Fuzzy Energy Management Strategy for PEM Fuel Cell–Battery–Supercapacitor Hybrid Excavator

Hoai Vu Anh Truong ¹, Hoang Vu Dao ¹, Tri Cuong Do ¹, Cong Minh Ho ¹, Xuan Dinh To ¹, Tri Dung Dang ¹ and Kyoung Kwan Ahn ^{2,*}

¹ Graduate School of Mechanical and Automotive Engineering, University of Ulsan, Daehakro 93, Nam-gu, Ulsan 44610, Korea; truonganh241292@gmail.com (H.V.A.T.); hoangvudaocsp@gmail.com (H.V.D.); cuongdt298@gmail.com (T.C.D.); hocongminhck@gmail.com (C.M.H.); pageplan33286@gmail.com (X.D.T.); dangtridungs@gmail.com (T.D.D.)

² School of Mechanical and Automotive Engineering, University of Ulsan, Ulsan 44610, Korea

* Correspondence: kkahn@ulsan.ac.kr; Tel.: +82-52-259-2282

Received: 18 April 2020; Accepted: 28 June 2020; Published: 1 July 2020



Abstract: By replacing conventional supplies such as fossil fuels or internal combustion engines (ICEs), this paper presents a new configuration of hybrid power sources (HPS) based on the integration of a proton-exchange membrane fuel cell (PEMFC) with batteries (BATs) and supercapacitors (SCs) for hydraulic excavators (HEs). In contrast to conventional architectures, the PEMFC in this study functions as the main power supply, whereas the integrated BAT–SC is considered as an auxiliary buffer. Regarding shortcomings existing in the previous approaches, an innovative energy management strategy (EMS) was designed using a new mapping fuzzy logic control (MFLC) for appropriate power distribution. Comparisons between the proposed strategy with available approaches are conducted to satisfy several driving cycles with different load demands and verify the strategy’s effectiveness. Based on the simulation results, the efficiency of the PEMFC when using the MFLS algorithm increased up to 47% in comparison with the conventional proposed EMS and other approaches. With the proposed strategy, the HPS can be guaranteed to not only sufficiently support power to the system even when the endurance process or high peak power is required, but also extend the lifespan of the devices and achieves high efficiency.

Keywords: modeling of PEMFC; EMS for hybrid PEMFC; rule-based EMS; fuzzy logic system

1. Introduction

Hydraulic excavators (HEs) are essential to construction and agriculture [1–11], however, existing issues such as low energy efficiency and carbon emissions in HEs using an internal combustion engine (ICE) have urgently imposed alternative energy requirements with the aim of reducing environmental and economic problems. In the trend of exploring and developing alternative power sources to take the place of fossil fuels, the proton-exchange membrane fuel cell (PEMFC) has become a potential candidate due to its high performance in high energy conversion efficiency, low chemical pollution, quiet operation, low weight, and low volume, especially in producing zero-emissions. However, low power density and slow power response are drawbacks of the PEMFC. Moreover, transient change in the load demand due to complicated requirements or working terrains is difficult to adequately satisfy using the standalone PEMFC. Furthermore, when the HEs are in regeneration modes or when the PEMFC releases more power than the demand, the PEMFC itself is not able to store the excess energy. A power deficiency when increasing the operating load and the waste power in the case of regeneration mode require at least one auxiliary device to enhance and optimize performance.

The first integrated configuration was reported by Yi et al. [12]. In his study, the integration of a fuel cell (FC) with batteries (BATs) was proposed as a power source for the HEs based on workload. The BAT is expected to be remarkably ideal and supportive storage in HEs. Nevertheless, the required hydraulic power in this paper indicates an abrupt and un-cyclical power demand under workloads of placing soil and putting it down after the HE has completed a slewing motion. In practice, HEs have to complete many combinations of motion (e.g., lifting, moving, rotating, braking, and auxiliary systems), which also generates transient power loads. Consequently, the BATs cannot sufficiently adapt in the case of rapidly changing power. Gong et al. [13] proposed the integration of the FC with an ultra-capacitor and derived a strategy to minimize an equivalent fuel consumption. Li et al. [14] proposed a suggested configuration comprising the PEMFC integrated with supercapacitors (SCs) for construction machines and developed an algorithm for an energy management system (ems) strategy that relies on model predictive control (MPC) [15]. The results indicated that this configuration could effectively adapt to the system operation and the state of charge (SoC) of the SCs could be maintained in good condition. Based on these approaches, Li et al. improved his algorithm and applied it to an excavator with the same configuration as the integrated power source [16]. Although the above works revealed that good results can be achieved, the SC cannot sufficiently supply energy when a high load power requires endurance missions regarded the SC characteristics, as presented in [17]. Accordingly, the SC is suitable when a large amount of power is required to support and absorb the transient peak power, whereas the BAT is capable of storing large amounts of energy and is useful for sustaining energy in the long term. Therefore, the use of the BAT–SC is more efficient than using segregated equipment, thus increasing workability and system reliability. The integration of BAT–SC with the PEMFC can achieve a higher performance, reduce system size, and minimize the fuel economy cost. Nevertheless, another issue arising from integrating the three devices is how to effectively manage the complex HPS. Thus, the design of an energy management strategy (EMS) is required to split the energy from the powertrain and appropriately distribute it to other components.

The literature on lightweight hybrid electric vehicles [18–23] provide helpful references for effectively delivering power between the components of the integrated system using the EMS. In [18], Vanessa et al. formulated a strategy in which the FC functioned as a primary source, whereas the BAT and SC functioned as buffer supplies. The order of using each component was explained by a flowchart in which the state of charge of each device was considered critically. In [19], Aya et al. expressed two configurations for vehicles: the hydrogen fuel-saving control strategy (HFS-CS) and the life cycle saving control strategy (LCS-CS). However, according to the two flowcharts, instability due to overcharging in each device or a lack of power in both SC and BAT can occur because the order of use is not appropriate. Zhang et al. suggested a strategy for the hybrid FC–BAT–SC power-sharing on a tram [20]. As obtained from the literature, most of those studies have focused on sketching the EMS in flowchart form without considering the change phase between the different modes. This implies that all components can be operated by switching modes (simply ON/OFF) to satisfy specific conditions. This may cause a delay to the system and cause instability due to sudden change, thereafter degrading the performance of the devices over time. Based on the fact that the status change of devices (especially for the FC and BAT, which have slow dynamics responses) requires a certain time to meet the demanded tasks, this is not feasible when simply embedding these flowcharts into real test benches. Consequently, many studies have been implemented to overcome this drawback.

A fuzzy logic control (FLC) has been highlighted as a powerful tool to work out the complex issues concerning system logic. The use of the FLC was first suggested by Agustín et al. [24]. In his study, FLC was employed to split power for each device. The inputs of the FLC included the power required, SC state of charge (SoC_{SC}), and BAT state of charge (SoC_{BAT}), and the output was the demanded power for the PEMFC and BAT. The rules specified in the FLC were designed by following specific criteria. In [25], Li et al. proposed using FLC for energy and battery management in a series of hybrid electric vehicles. The study indicated that using FLC could constrain the system so that it operated within the fuel economic region and avoided the over-discharge of the BAT. In [26], Li et al.

employed the FLC to manage power-sharing between three different sources and guarantee their performance. The simulations were implemented in four standard driving cycles and the results proved that the suggested algorithm could satisfy the power demanded in comparison with other methods. Using the advantages of FLC, Issam et al. applied this technique for the EMS used in stand-alone applications [27]. Another application was introduced by Fei et al. when a master–slave EMS-based fuzzy logic hysteresis state machine was exploited for power split management applied to a PEMFC–lithium battery–supercapacitor (PEMFC–LIB–SC) hybrid tramway powertrain system [28]. Saman et al. [29] utilized fuzzy rules combined with a genetic algorithm (GA) to improve the vehicle’s dynamic performance of the hybrid FC–BAT–SC system and fuel economy. As the author claimed, the study contributed to related research from different aspects. Summarizing from previous approaches, Yakup et al. realized an analysis and comparison of several control methodologies for fuel-saving in hydrogen fuel cell vehicles integrated with BAT and SC [30]. In [31], Zhang et al. conducted an investigation on unplugged electric vehicles (UEVs) by employing an online fuzzy for the power management of the HPS composed of the PEMFC and BAT, and presented the procedure for power split management. The power required from the FC was produced after being processed in the FLC. The pulsed-power profile was used to verify its effectiveness and stability to the rapid change of the instantaneous high-power demand. With a similar rule-based approach used in previous works, Cong et al. established a new on–off power following a strategy-based fuzzy algorithm for FC extended-range vehicles in which the BAT was employed as the main source while the FC was considered as an extender for the system [32]. The simulation demonstrated that good results and improvement could be accomplished in both system dynamics and economy. Eckert et al. [33] utilized GA to optimize the lower and upper values of the membership function to maximize system performance. In [34], Ameer et al. proposed a master–slave fuzzy algorithm to design the EMS to effectively manage a hybrid power system and prolong all component lifespans.

Based on the literature, the FLC that mimics human knowledge [35–37] is an appropriate tool for establishing the EMS and applying it to the complicated hybrid system. Despite achieving good performance, few studies have reported on an application of these accomplishments for HEs. Furthermore, due to mimicking designer knowledge, it is challenging to achieve a good performance without setting an appropriate value and condition for the fuzzy system. Optimization methods have been successfully applied for the experimental system; nevertheless, most configurations have been conducted in two-device configurations such as FC–BAT, FC–SC, and BAT–SC. When configurations of three devices are considered, the power-sharing strategies are more complicated. Although the FLC, known to mimic designer knowledge, is difficult to design, it is still a suitable solution for a power-sharing design of a hybrid FC–BAT–SC. This technique can cover all scenarios of the working operation and mutual influences of charging–discharging mode in BAT–SC to maintain the high performance of all components. Considering the advantages of the integration of FC–BAT–SC and a lack of algorithms when designing the EMS for HEs, this study proposed a novel algorithm in which the FLC is exploited as the EMS to appropriately distribute power to each component. Building on our previous work in [38], we focused on how to operate all components in an optimal condition as the prior criterion to increase efficiency, thus prolonging lifespan and reducing costs. In order to handle these problems, an optimal mapping FLC (MFLC) was systematically designed based on a self-tuning methodology to generate the optimized parameters of all devices, thus adjusting power-sharing. The contributions of this research are as follows:

- (1) With our experience in fluid power and construction HEs, we proposed a novel configuration for the integration of FC–BAT–SC and attempted to apply it to HEs. In contrast to the conventional configuration in which the BATs are considered as the main supply, in this configuration, the FC functions as the main power source, and the BAT–SC is attached as supplements.
- (2) A novel EMS strategy was introduced in which the MFLC was designed to match the optimal condition during operation. While FLC was employed to distribute sufficient power to each component under different scenarios, the mapping condition was first introduced to calculate

a suitable fuel cell power. This control scheme is the key point to addressing problems associated with HE power distribution, which are considered as constrained multi-objective problems. The effectiveness of the proposed algorithm was validated by the standard driving cycle in which all working operations of the HE were investigated.

- (3) The regenerative mode of the HEs is mentioned and the difficulty in designing power-saving transmission for regeneration is explained.
- (4) The dynamic model of the entire system comprising the HE and integrated power sources were derived in detail. This model was simulated in a co-simulation AMESim-MATLAB/Simulink environment. The HE model was simulated in the AMESim software, whereas the models of FC, BAT, and SC were derived and performed in a MATLAB/Simulink software. The goal of this study was how to establish a real-time EMS, achieve the demand of the powertrain, and stabilize the entire platform when highly-fluctuating power occurred.
- (5) Finally, comparisons between the proposed algorithm with other conventional approaches are discussed to verify the effectiveness of the new configuration compared to previous conventional approaches.

The rest of this paper is organized as follows: Section 2 expresses the modeling of all components. Based on the characteristics of each device, the new configuration and the proposed EMS with regeneration mode are introduced in Section 3. Section 4 describes the MFLC based on the proposed EMS to achieve high efficiency and performance. To verify its advantages, comparative simulations between the proposed and conventional EMSs are discussed in Section 5. Finally, Section 6 summarizes and presents potential future applications.

2. System Configuration and Devices Modeling

2.1. Hydraulic Excavator Configuration

The power demand for running the HE is simply based on the total power needed for moving each element as requirements, driving crawlers, and running the hydraulic circuit. In the entire hydraulic system as depicted in Figure 1, the total power is a product of the outlet pressure and the flow rate of the hydraulic pump [39]:

$$P_p = \frac{p(t) \times D \times n(t)}{600 \times \eta(t)} \quad (1)$$

$$P_M = \frac{P_p}{\eta_M} \quad (2)$$

where p , D , n , and η are the pressure (bar), displacement (l/rev), rotational speed (rev/min), and volumetric efficiency of the hydraulic pump, respectively. P_M is the computed motor power to drive the hydraulic pump (kW); η_M is an efficiency dropped when converting electric power to mechanical power.

The hydraulic circuit of the HE is inherited from the AMESim library and described in Figure 1 [40].

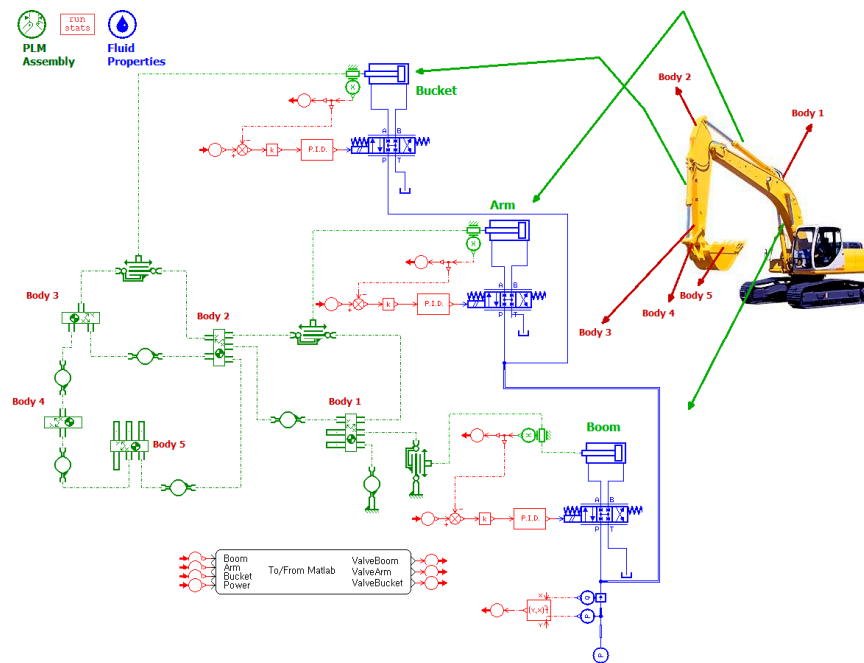


Figure 1. Excavator AMESim hydraulic model.

2.2. Fuel Cell Modeling

The PEMFC model is referred to in [41–45]. The dynamics of a single fuel cell is calculated as follows:

$$V_{cell} = E_{Nernst} - V_{act} - V_{conc} - V_{ohmic} \quad (3)$$

$$E_{Nernst} = 1.229 - 8.5 \times 10^{-4}(T - 298.15) + \frac{RT}{2F} \ln[p'_{H_2}(p'_{O_2})^{0.5}] \quad (4)$$

$$V_{ohmic} = iR_{int} \quad (5)$$

$$V_{act} = \xi_1 + \xi_2 T + \xi_3 T \ln(c'_{O_2}) + \xi_4 T \ln(i) \quad (6)$$

$$V_{conc} = \frac{RT}{nF} \ln\left(\frac{(i/A)_L}{(i/A)_L - (i/A)}\right) \quad (7)$$

where E_{Nernst} , V_{act} , V_{conc} , and V_{ohmic} are voltage losses of the thermodynamic potential, activation process, concentration, and ohmic voltage loss, respectively. p'_{H_2} , p'_{O_2} , T , R , and F represent the hydrogen and oxygen partial pressure, cell temperature, universal gas constant, and Faraday constant, respectively. R_{int} is the internal resistance of the electrolyte membrane; c'_{O_2} is the oxygen concentration at the cathode/membrane interface; $\xi_1 \dots \xi_4$ are parametric coefficients; and i is the cell current [38].

Due to the double capacitor layer effect at the electrode–electrolyte interface, the voltage drop can be computed as [46]

$$\frac{dV_d}{dt} = \frac{i}{C_{dl}} - \frac{V_d}{R_d C_{dl}} \quad (8)$$

$$R_d = \frac{V_{act} + V_{conc}}{i} \quad (9)$$

where R_d is the activation resistance and concentration resistance, and V_d is the voltage drop.

The voltage of a single cell and total voltage when combining the number of cells N can be computed as

$$V_{cell} = E_{Nernst} - V_d - V_{ohmic} \quad (10)$$

$$V_{stack} = NV_{cell} \quad (11)$$

On the anode-side, the reactant flow model is given by the following:

$$\frac{V_a}{RT} \frac{dp'_{H_2}}{dt} = \dot{m}_{H_2,in} - \dot{m}_{H_2,out} - \frac{Ni}{2F} \quad (12)$$

$$\dot{m}_{H_2,out} = k_a(p'_{H_2} - p_{\text{tank}}) \quad (13)$$

$$\frac{V_c}{RT} \frac{dp'_{O_2}}{dt} = \dot{m}_{O_2,in} - \dot{m}_{O_2,out} - \frac{Ni}{4F} \quad (14)$$

$$\dot{m}_{O_2,out} = k_c(p'_{O_2} - p_{BPR}) \quad (15)$$

$$P_{tot} = \dot{m}_{H_2,used} \Delta H = \frac{Ni}{2F} \Delta H \quad (16)$$

where $V_a, \dot{m}_{H_2,in}, \dot{m}_{H_2,out}$ are the anode volume, hydrogen inlet, and outlet flow rates through the fuel cell (FC) stack, respectively. k_a is a flow constant for the anode, and p_{tank} is the pressure of the hydrogen tank. $V_c, \dot{m}_{O_2,in}, \dot{m}_{O_2,out}$ are the cathode volume, oxygen inlet, and oxygen outlet flow rate through the FC stack, respectively. k_c and p_{BPR} are the flow constant in the cathode and oxygen pressure at the outlet, respectively. P_{tot} denotes a total power input of the system, which changes linearly with hydrogen consumed, and ΔH is the hydrogen enthalpy of combustion.

Finally, the electrical output power can be obtained as

$$P_{elec} = V_{stack} i \quad (17)$$

2.3. Supercapacitor Modeling

The SC was selected as the first support unit to supply different power between the demand and power generated from the FC and BATs in the case of sudden change due to its advantages such as high power density, fast charge, and high release power. Without using a SC, the FC and BATs have to manage the entire required workload even when high peak power happens, thus degrading lifespan, or increasing the size and costs in a trade-off [47]. Moreover, as Phatiphat stated in [48], when the time constant is less than 0.1 s, energy cannot be obtained from the same sized BAT, but the SC can totally provide energy at a very high rate. This is the highlighted advantage of the SC. Many different models have been suggested using the RC circuit. The equivalent SC model can be referred to in [48–50]. Naturally, the SC consists of capacitors and resistors that represent the charging and discharging units, and an equivalent parallel resistor is the self-discharging loss [51]. The unit cell of the SC was constructed with two RC branches in a parallel manner, as presented in Figure 2 [52].

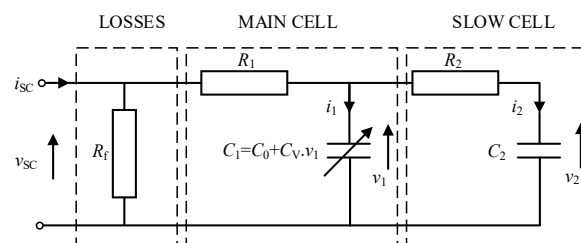


Figure 2. A simplified model of the supercapacitor.

As depicted in Figure 2, the main cell, $R_1 C_1$, specifies the immediate response during the charge or discharge process within a short time duration [53]. All charged energy is in the capacitor C_1 of the immediate branch at the end of the charging mode. Then, the charge re-splits itself to the second slow cell, $R_2 C_2$. The resistor R_f denotes a leakage behavior based on the fact that there always exists

a leakage current flow of the SC during a self-discharge phenomenon [54]. This current leakage is approximately several milliamps in a large SC. The model of SC is derived as

$$U_{sc} = N_{s_sc} \left(v_1 + R_1 \frac{I_{sc}}{N_{p_sc}} \right) \quad (18)$$

$$i_1 = C_1 \frac{dv_1}{dt} = \frac{dQ_1}{dt} = (C_0 + C_v v_1) \frac{dv_1}{dt} \quad (19)$$

$$Q_1 = C_0 v_1 + \frac{1}{2} C_v v_1^2 \quad (20)$$

$$i_1 = i_{sc} - i_2 \quad (21)$$

$$v_2 = \frac{1}{C_2} \int \frac{1}{R_2} (v_1 - v_2) dt \quad (22)$$

$$Q_2 = \int i_2 dt \quad (23)$$

where U_{sc} and I_{sc} are the voltage and current of the pack SCs; and v_{sc} and i_{sc} are the voltage and current of an elementary SC. N_{s_sc} and N_{p_sc} denote the number of SCs in a serial connection and the number of parallel branches, respectively. i_1 and i_2 are the current through the main cell and the slow cell. Q_1 and C_1 are the instantaneous charge state of the main cell. v_1 , v_2 is the voltage of the first and secondary branches. Q_2 and C_2 are the instantaneous charge states of the slow cell.

Finally, the SoC_{SC} is an important parameter to evaluate the state of the SC bank for designing the EMS. The change rate of the SoC_{SC} is proportional with the charging current i_{sc} [55]:

$$\frac{d}{dt} SoC_{SC} = \frac{i_{sc}}{Q_{SCmax}} \quad (24)$$

where Q_{SCmax} denotes the maximum capacity of the SC.

2.4. Battery Modeling

The BAT is the second buffer supply for the system when the FC and/or the SC cannot maintain the workload demand during the endurance process. The BAT model is constructed with specific invoked parameters to evaluate its working status, thereby establishing criteria for effectively initializing the EMS. The BAT model used in this study follows the circuit proposed in [56].

$$E = E_0 - K_{BAT} \frac{Q_{BATmax}}{Q_{BAT}} + A_{BAT} e^{B(Q_{BAT} - Q_{BATmax})} \quad (25)$$

$$\begin{aligned} V_{bat} &= E - R_{BAT} i_{BAT} \\ P_{BAT} &= V_{BAT} i_{BAT} \end{aligned} \quad (26)$$

$$Q_{BAT} = Q_{BAT}(t_0) - \int_{t_0}^t i_{BAT} d\tau \quad (27)$$

where E is the controlled voltage source; V_{BAT} and P_{BAT} are the BAT voltage and output power, respectively; Q_{BAT} and Q_{BATmax} denote the instant and maximum BAT capacity, respectively; i_{BAT} is the load current; and t is time parameterized. A_{BAT} is an exponential zone amplitude (V).

The SoC_{BAT} can be derived from the current charge and the maximum charge of it.

$$SoC_{BAT} = \frac{Q_{BAT}}{Q_{BATmax}} \quad (28)$$

The SoC_{BAT} is another important parameter, along with the SoC_{SC} , that reveals the device status and is invoked to assess the available energy remaining. The direction of the current determines the charge or discharge mode of the BAT. Compared with the BAT model in [47,57,58], this model gives the shortened form and can be used in both charge and discharge mode without losing its characteristics.

2.5. DC/DC Converter Modeling

For the studied hybrid electric excavator system, the BAT and SC were interfaced with the DC bus by using a bidirectional DC/DC converter, which can allow energy flow in both directions. The PEMFC system was linked with the DC bus via a buck DC/DC converter, which can adapt the voltage level of the DC bus. These DC/DC converters are the crucial execution devices of the energy management process, which can regulate an output voltage and current using a local controller. The energy management process is at a higher level than a local controller of the DC/DC converters and it is assumed that the time constant of the inductors in the DC/DC converters are much greater than the switching period [59]. Therefore, once the inner-loop subsystem is well controlled, it can respond immediately to the reference. Thus, it is reasonable to reduce the fast dynamics of the DC/DC converter using the following equivalent static model [60,61].

$$V_I - V_h = L \frac{di_L}{dt} + i_L R_L \quad (29)$$

$$V_h = \kappa_{DC} V_O \quad (30)$$

$$i_O = \kappa_{DC} i_L \eta_{DC}^\varepsilon \quad (31)$$

where V_I , V_O are the DC/DC converter input and output voltage, respectively; R_L is the resistor of the inductor and L is its inductance; κ_{DC} is the ratio of converter output and input voltage; i_L and i_O are currents through the inductor and the output current of the converter, respectively; η_{DC} is the converter efficient; $\varepsilon = 1$ for boost mode or the bidirectional mode with $i_O V_O \geq 0$ and $\varepsilon = -1$ for bidirectional mode when $i_O V_O < 0$.

3. Configuration and Proposed Energy Management Strategy (EMS) for the Hydraulic Excavator

3.1. Hybrid Power Hydraulic Excavators Configuration

The hybrid power HE (HP-HE) was constructed as depicted in Figure 3a, in which the ICEs were alternatively replaced by the hybrid FC-BAT-SC power source and electric motor. The entire system can be considered as the HPS associated with the hydraulic actuators (HAs) through the DC bus. The HPS comprises the PEMFC functioning as the primary supply and the BAT-SC functioning as auxiliary buffers. The goal of the HPS is to supply power as the load power required and store energy in the case of regeneration. The power induced from the HPS provides power to the electric motor through DC/DC converters, and the electric motor drives the practical hydraulic system. The HAs consisted of three hydraulic cylinders for the driving boom, arm, and bucket, and one swing hydraulic motor for driving the HE body. The movement of the three cylinders was distinguished by using a main control valve block to control the flow rate to each actuator. Furthermore, the HAs were extended by the regeneration part to recover the energy-saving when the boom automatically moves down due to gravity, as shown in Figure 3b.

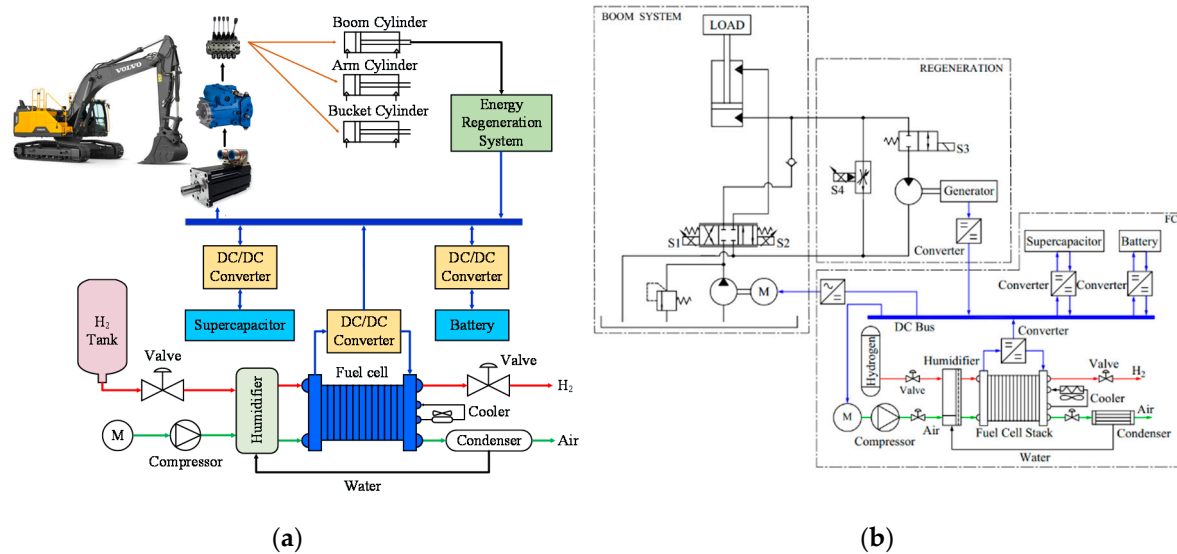


Figure 3. The structure of the new configuration: (a) hybrid power hydraulic excavators (HEs) and (b) hydraulic circuit for boom energy regeneration part.

3.2. Proposed Energy Management Strategy (EMS)

Based on the fact that HEs perform various functions such as digging, lifting soil, spinning, ground leveling, and so on, an EMS was proposed to productively achieve the requirements. Improving the system performance and considering regeneration mode for saving energy were taken into consideration. From the requested motions of the excavator, the power required (P_{red}) was determined as a reference for running the power from the HPS. The SoC_{BAT} and the SoC_{SC} were used to evaluate the state of the components. Furthermore, the minimum SoC signed by SoC_{BAT_min} and SoC_{SC_min} was used to monitor when the two devices needed to be charged. The flowchart of the proposed EMS is depicted in Figure 4.

As depicted in Figure 4, in the beginning, the power required was examined to determine if its value was negative. In this case, the HE is moving downhill, when the swing is braking after spinning the entire body, or when the boom is moving down, whereas other elements do not operate. When these events happen, the BAT-SC is not required to release power. Instead, depending on the level of the power-saving, the FC is switched OFF or runs in an optimal value in which the highest efficiency can be achieved to charge the BAT-SC.

Otherwise, when P_{req} is positive, the following circumstances should be considered. If the power demand is less than the nominal power of the FC (P_{fc_n}), the FC primarily supplies power to the system and charges the auxiliary supplements for later use. The charging is stopped if the SoC_{BAT}/SoC_{SC} reaches the maximum value ($SoC_{BAT}/SoC_{SC} = SoC_{Max}$). If the load demand exceeds the FC nominal power, the combination between the FC and BAT or SC is considered, if their power can sufficiently satisfy the load demand. This scenario is highlighted in light blue and light green in Figure 4. The combination of FC-SC is considered in the case when the BAT cannot satisfy the sudden change in power required, as explained in the SC modeling part. Otherwise, the prior combination of FC-BAT is used. During this process, if the SoC_{BAT} (or SoC_{SC}) drops to the minimum level, the SC (or BAT) is alternatively used, and the other device is alarmed and switched to charge mode. If the P_{req} exceeds the combination of FC-BAT (or FC-SC), all devices enter together and provide power to the system. During these processes, the SoC_{BAT} and SoC_{SC} should be monitored and the SC is always charged first.

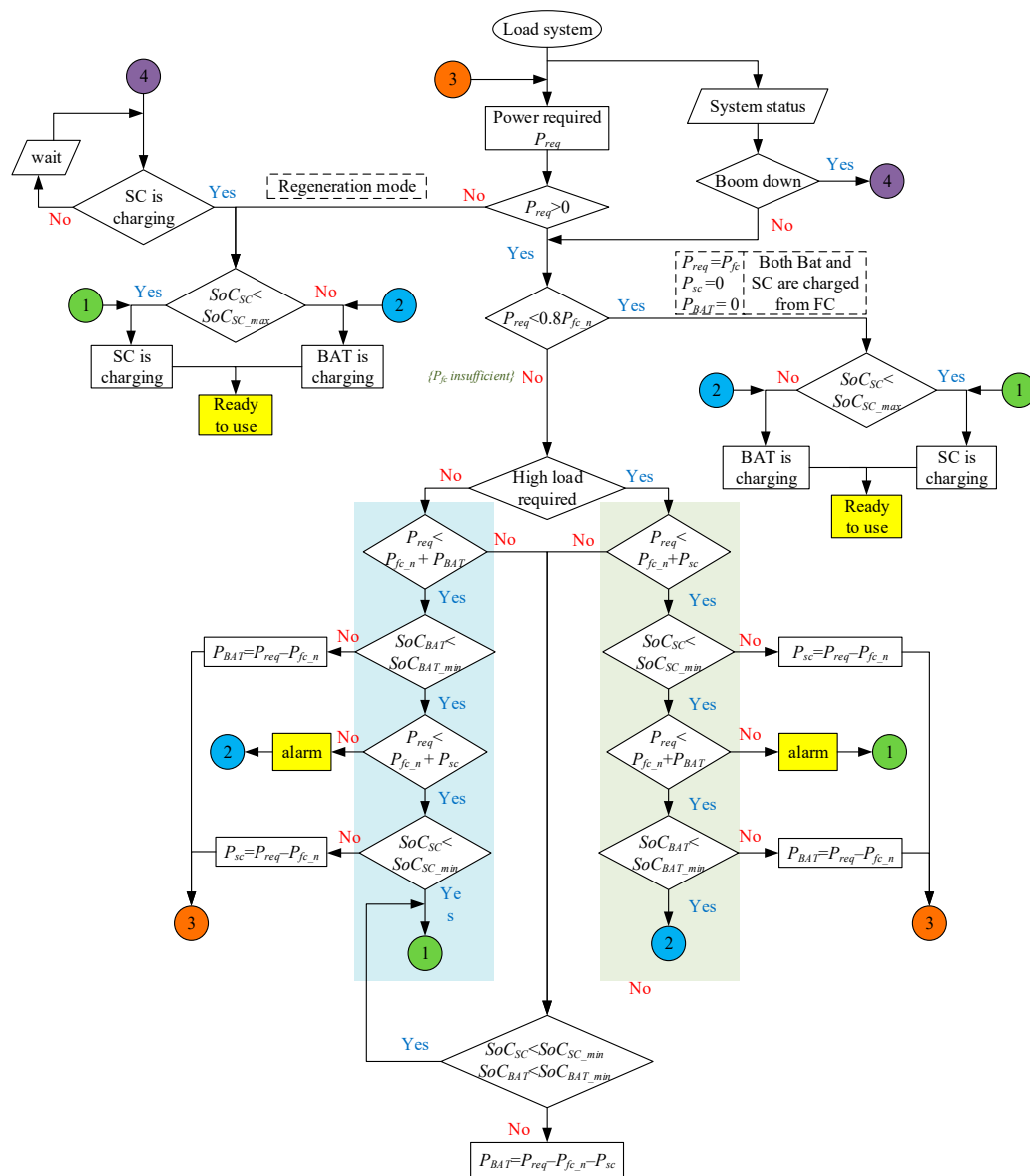


Figure 4. The proposed strategy for energy management strategy (EMS) with the regeneration part.

3.3. Regeneration Mode

In electric vehicles (EVs), the charge mode occurs when the cars are moving downhill or braking, while the FC is still supplying power to the system. One important point to clarify is that the charge and discharge mode cannot simultaneously occur as analyses in conventional algorithms. Since the BAT–SC is connected with only one engine and the engine is directly coupled with two-back-wheels, by using bi-directional DC/DC converters in the hybrid source, the state of the devices can be easily switched to capture or release power, depending on the state of the system and can be used in the same transmission line.

In contrast to the EVs, the powertrain of the HEs consists of various links (boom, arm, bucket, swing, and crawlers). Therefore, designing the regeneration mode in the HEs is more complicated than that of the EVs. We need to consider a case when one link is in a power-saving procedure (for instance, the boom is moving down automatically due to gravity), while the others continuously operate as usual. This implies that the power sources supplying progress for the system and power-saving progress from one or more elements occur at the same time. Hence, we cannot apply the same design as that of

the EVs. For general hydraulic circuits, one sub-system should be connected as the second line for saving energy. Consequently, in this design, the circuit diagram for hybrid sources is separated into two distinguished transmission lines: one for supply and one for regeneration. The power captured from the generation is transmitted through the second transmission line.

4. Fuzzy EMS for the Integrated System

According to the working principle presented by the above flow chart, the power obtained from the driving cycle can be separated into four cases: high power, medium power, low power, and regenerative mode. The conventional EMS can simply be considered as an on–off switch between devices. However, this method may generate a delay to the system, as explained in the Introduction. In practice, the change in the status of devices requires a certain time to achieve and adapt to the required tasks. This problem can be handled by employing a FLC, which is known to be a useful tool to split and distribute power. This method was previously suggested by [18]. In this approach, the prior SoC_{SC} is retained so that the stability of the SoC_{SC} is maintained in an acceptable condition. However, in practice, maintaining the SoC_{SC} in an acceptable condition is not as important as that of BAT due to its specification. In large systems that always work under high power for an extended period, the BAT operation and its status should be regulated so that its SoC exhibits variation or is prevented from dropping down to a very low value as a solution to prolong life-time. The efficiency curve of the PEMFC is shown in Figure 5.

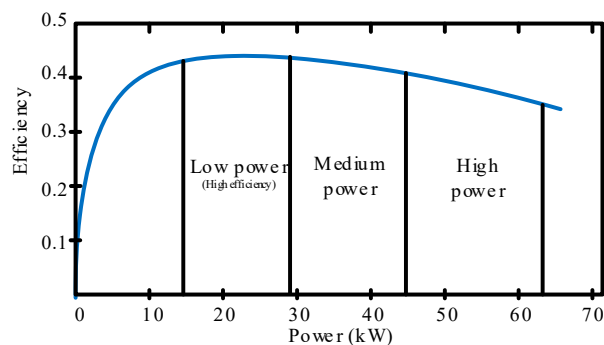


Figure 5. Fuel cell efficiency versus power.

As shown in Figure 5, efficiency does not increase as power increases. High power achievement requires more energy from the auxiliary devices (cooling or heating system), thus reducing the overall efficiency of the system. Therefore, designing an algorithm to maintain high efficiency when operating the FC is practically prioritized as the main criterion. Thereby, we can reduce hydrogen consumption and limit the on/off cycles of the system to extend lifespan. The FLS was set up with the following criteria to satisfy the above analysis:

- Increase the FC efficiency and minimize hydrogen consumption.
- The SoC_{BAT} should be frequently maintained within the range of 0.5~0.9 as a solution to prolong lifespan.
- The SoC_{SC} should be maintained at a high level to boost the power in the case of an emergency.

Therefore, the fuzzy control rules can serve to map the input linguistic variables P_{req} , SoC_{BAT} , and SoC_{SC} to the output linguistic variables P_{fc} , P_{BAT} , and P_{SC} , respectively. The input linguistic P_{req} is characterized by four membership functions as four levels of operation. The input linguistics SoC_{BAT} and SoC_{SC} are characterized by five membership functions (L (Low), ML (Medium–low), M (Medium), MH (Medium–high), H (High)). The output linguistics of the FC- P_{FC_ref} are characterized by four membership functions (O (Off), L (Low), M (Medium), H (high)), whereas the output P_{BAT} is a gain distributed within $[-1,1]$ interval and characterized by nine membership functions (NVB (Negative

Very Big), NB (Negative Big), NM (Negative Medium), NS (Negative Small), Z (Zero), PS (Positive Small), PM (Positive Medium), PB (Positive Big), PVB (Positive Very Big)). The matrix rules in the four cases are expressed in Tables 1–4. The membership function of the inputs and outputs are described in Figure 6.

Table 1. High power required.

P_{high}		$SoC_{SC} (0.2\sim0.9)$											
		$P_{fc_ref} P_{BAT}$		L		ML		M		MH		H	
$SoC_{BAT} (0.5\sim0.9)$	L	H	PS	H	PS	H	PS	H	PS	H	PS	H	PS
	ML	H	PB	H	PB	H	PB	H	PM	H	PM	H	PM
	M	H	PB	H	PB	H	PB	H	PM	H	PM	H	PM
	MH	H	PVB	H	PVB	H	PVB	H	PVB	H	PVB	H	PVB
	H	H	PVB	H	PVB	H	PVB	H	PVB	H	PVB	H	PVB

Table 2. Medium power required.

P_{med}		$SoC_{SC} (0.2\sim0.9)$											
		$P_{fc_ref} P_{BAT}$		L		ML		M		MH		H	
$SoC_{BAT} (0.5\sim0.9)$	L	H	Z	H	NS	H	NM	H	NB	M	NB	M	NB
	ML	H	PS	H	Z	H	NS	M	NM	M	NM	M	NM
	M	H	PM	H	PS	M	Z	M	NS	M	NS	M	NS
	MH	H	PB	M	PM	M	PS	M	Z	M	NS	M	NS
	H	M	PVB	M	PB	M	PM	M	PS	M	NS	M	Z

Table 3. Low power required.

P_{low}		$SoC_{SC} (0.2\sim0.9)$											
		$P_{fc_ref} P_{BAT}$		L		ML		M		MH		H	
$SoC_{BAT} (0.5\sim0.9)$	L	H	Z	H	NS	H	NM	H	NB	M	NB	M	NB
	ML	H	PS	H	Z	H	NS	M	NM	L	NM	L	NM
	M	H	PM	H	PS	M	Z	L	NS	L	NS	L	NS
	MH	H	PB	M	PM	L	PS	L	Z	L	NS	L	NS
	H	M	PVB	L	PB	L	PM	L	PS	L	NS	L	Z

Table 4. Regeneration mode.

$P_{fc_ref} P_{BAT} P_{sc}$			$SoC_{SC} (0.2\sim0.9)$													
			L		ML		M		MH		H					
$SoC_{BAT} (0.5 \sim 0.9)$	L	Opt. value	NS	NVB	Optimal value	NS	NVB	Optimal value	NM	NVB	Optimal value	NB	NM	Opt. value	NVB	NS
	ML	Opt. value	NS	NVB	Optimal value	NS	NVB	Optimal value	NS	NVB	Optimal value	NM	NM	Opt. value	NB	NS
	M	Opt. value	Z	NVB	Optimal value	Z	NVB	Optimal value	NS	NVB	Optimal value	NS	NM	O	NM	Z
	M	Opt. value	PS	NVB	Optimal value	PS	NVB	Optimal value	Z	NVB	O	NS	NM	O	NS	Z
	H	Opt. value	PM	NVB	Optimal value	PM	NVB	O	PS	NVB	O	Z	NM	O	NS	Z

For the regeneration mode, because the excavator does not require any power from the power supply, the power of the FC is adjusted to operate at maximum efficiency in the case of charging auxiliary devices when the SoC drops down to a low value and off when the SoC level is high. Furthermore, the power of BAT and SC power are assigned as outputs of the FLC. The fuzzy rule of the regenerative mode is presented in Table 4.

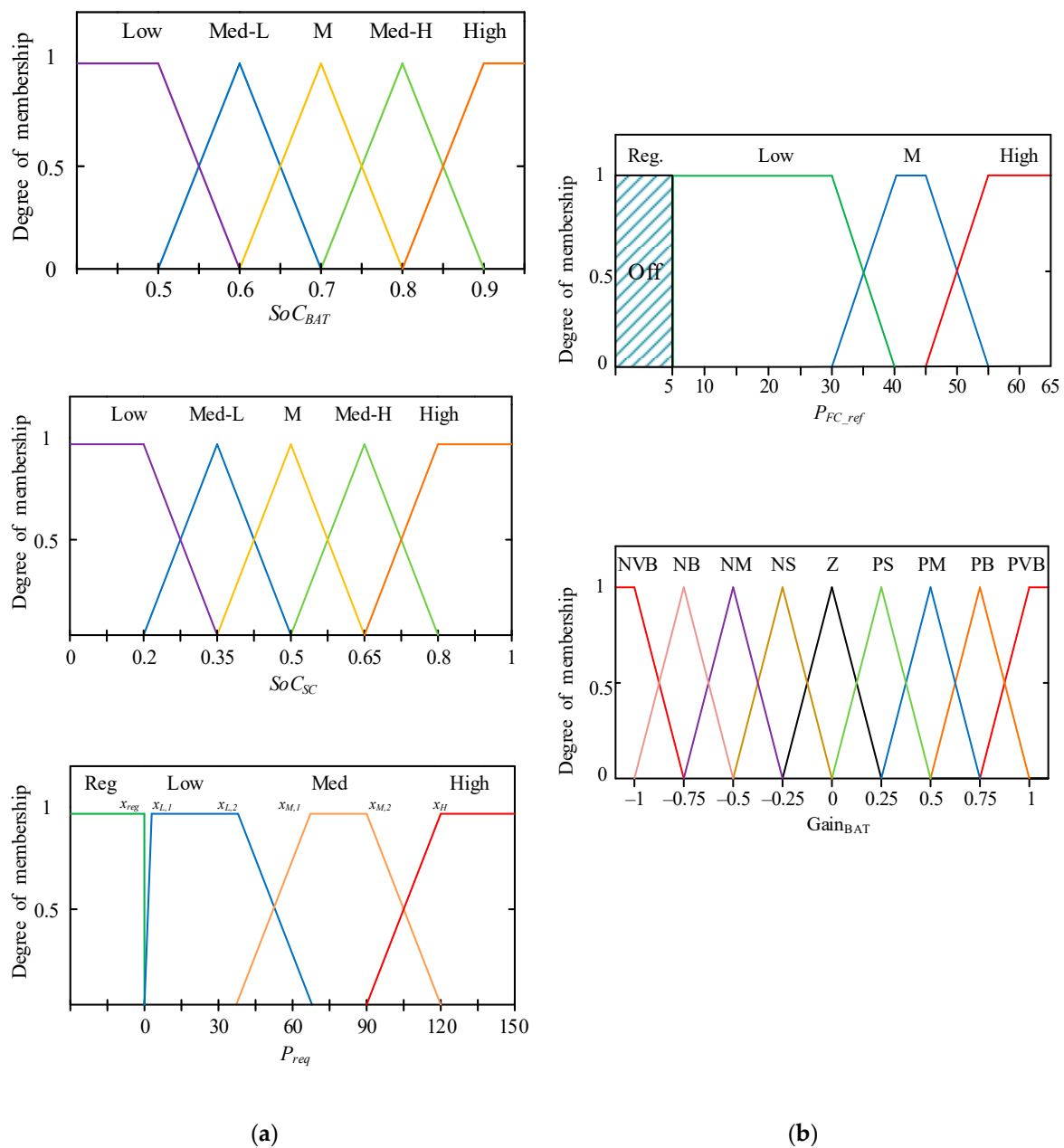


Figure 6. Structure of the FLS: (a) membership functions of inputs and (b) membership functions of outputs.

In this study, triangular membership functions are exploited as depicted in Figure 6. The left side illustrates the inputs of the FLS in which the power required P_{req} , SoC_{BAT} , and SoC_{SC} are considered; the right side is the product including the FC power and gains of the BAT for charging or discharging mode. Additionally, to match the aforementioned criteria, the four following requirements should be satisfied:

- In the case of low devices SoC (SoC_{BAT} and SoC_{SC} are low), the FC power can be set up to a high value for quick charging, even when the system is operating with medium or low power required.
- For medium and low power required, if the SoC_{BAT} is greater than medium level, the BAT charges the SC instead of using FC; therefore, the FC does not need to run at a high value, and the efficiency can be increased consequently.

- In the case of charging, the SC is always charged so that a good condition of the SoC_{SC} can be maintained for later use.
- The final goal is to force the FC power to the highest efficiency point, as shown in Figure 5.

The completed control schematic diagram is depicted in Figure 7.

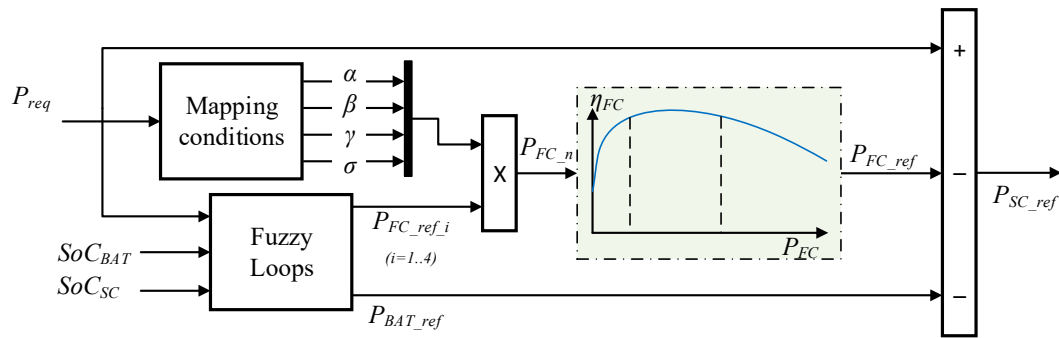


Figure 7. Control schematic diagram for power distribution.

Since the power of the system in some cases can be referred to as the mixture between two cases, (for instance, if the required power is 85 kW, then this value can belong to both high power and medium power), then the scheduling gains is used to calculate the exact output power of the FLC. Let us define the vector $K = (\alpha \ \beta \ \gamma \ \sigma)^T$ as the gains of the high power, medium power, low power, and regenerative power, respectively. Then, the output power is calculated as:

$$P_{FC}^* = K^T P_{FC}^* = \alpha P_{FC1}^* + \beta P_{FC2}^* + \gamma P_{FC3}^* + \sigma P_{FC4}^* \tag{32}$$

where $P_{FC}^* = (P_{FC1}^* \ P_{FC2}^* \ P_{FC3}^* \ P_{FC4}^*)^T$ is an output of the four FLC, respectively, $K = (\alpha \ \beta \ \gamma \ \sigma)^T$ is calculated as:

$$\left\{ \begin{array}{l} K = (\alpha \ \beta \ \gamma \ \sigma)^T = (0 \ 0 \ 0 \ 1)^T \quad \text{if } P_{req} \leq x_{reg} \\ K = (\alpha \ \beta \ \gamma \ \sigma)^T = (0 \ 0 \ 1 \ 0)^T \quad \text{if } x_{L,1} \leq P_{req} \leq x_{L,2} \\ \left\{ \begin{array}{l} \alpha = 1 - \text{sat}\left(\frac{|x_H - P_{req}|}{x_H - x_{M,2}}\right) \\ \beta = 1 - \text{sat}\left(\frac{|x_{M,1} - P_{req}|}{x_{M,1} - x_{L,2}}\right) \times \frac{|\text{sign}(x_{M,1} - P_{req}) - \text{sign}(x_{L,2} - P_{req})|}{|\text{sign}(x_{M,1} - P_{req})| + |\text{sign}(x_{L,2} - P_{req})|} \\ \quad - \text{sat}\left(\frac{|x_{M,2} - P_{req}|}{x_H - x_{M,2}}\right) \times \frac{|\text{sign}(x_{M,2} - P_{req}) - \text{sign}(x_H - P_{req})|}{|\text{sign}(x_{M,2} - P_{req})| + |\text{sign}(x_H - P_{req})|} \\ \gamma = 1 - \text{sat}\left(\frac{|x_{L,2} - P_{req}|}{x_{M,1} - x_{L,2}}\right) \end{array} \right. \quad \text{Otherwise} \\ K = (\alpha \ \beta \ \gamma \ \sigma)^T = (0 \ 1 \ 0 \ 0)^T \quad \text{if } x_{M,1} \leq P_{req} \leq x_{M,2} \\ K = (\alpha \ \beta \ \gamma \ \sigma)^T = (1 \ 0 \ 0 \ 0)^T \quad \text{if } P_{req} \geq x_H \end{array} \right. \tag{33}$$

Consequently, the FC power used for the net is computed as

$$P_{FC_net} = \eta_{FC} P_{FC}^* \tag{34}$$

5. Numerical Simulation and Discussion

5.1. Parameters Setup for Simulation

In this section, the simulations and comparisons between the proposed control strategy with previous approaches are examined to evaluate the effectiveness of the proposed HPS under different

working conditions. The simulations were conducted in a co-simulation between LMS AMESim 15.2 software and MATLAB/Simulink 2019a as depicted in Figure 8.

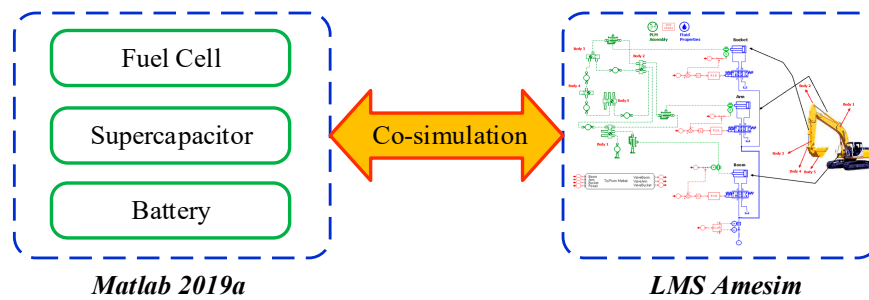


Figure 8. Co-simulation environment.

The LMS AMESim, known as specialized software for dynamic simulation with various applications, was employed to express the HE configuration. The parameters for simulating the HE are described in Table 5. The modeling of the HPS was deployed in MATLAB/Simulink, in which all mathematical equations were embedded, and the results were displayed with a sampling time of 10 ms. The component sizes of the HPS were reasonably chosen to satisfy the demand and verify the proposed methodology as listed in Tables 6–8. The testing trajectories of the boom, arm, and bucket of the excavator are described in Figure 9, and the required power from those motions is performed in Figure 10.

Table 5. Parameters for the excavator model.

Component	Value	Unit
Boom cylinder (Piston diameter × Rod diameter × Stroke length)	0.35 × 0.22 × 1.8	m
Arm cylinder	0.18 × 0.125 × 1.7	m
Bucket cylinder	0.21 × 0.13 × 1.33	m

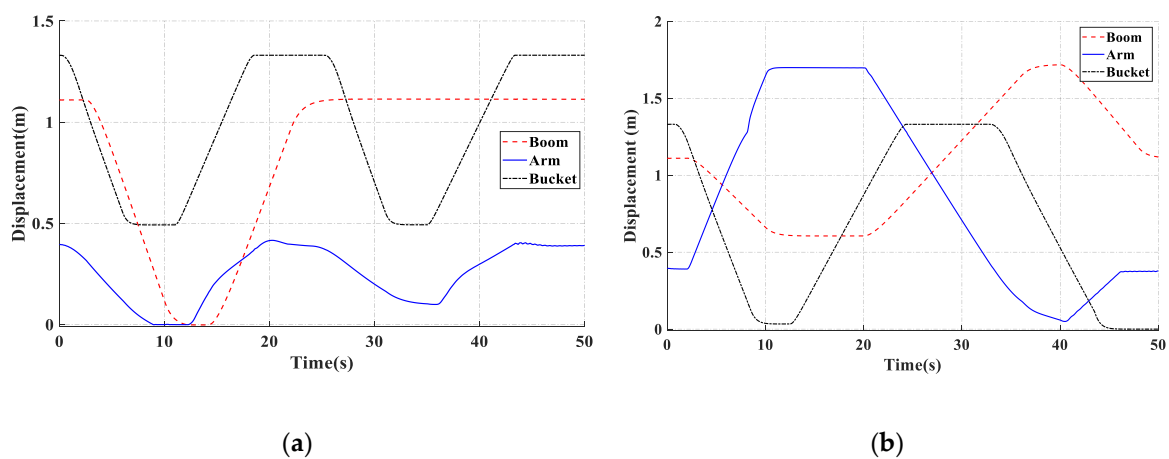


Figure 9. Excavator trajectories of the boom, arm, and bucket with two different working cycles: (a) trajectory 1; (b) trajectory 2.

Table 6. Fuel cell system parameters [38,41].

Parameter		Value	Unit
Number of cells	N	35	-
Number of stacks	-	18	-
Rated power	-	3.6	kW
Membrane thickness	-	178	μm
Anode pressure	p_{H2}	3	atm
Cathode pressure	p_{O2}	3	atm
Cell area	A	232	cm^2
Coefficients	ξ_1	-0.948	-
	ξ_2	$0.00286 + 2 \times 10^{-4} \times \ln(A)$ $+ 4.3 \times 10^{-5} \times \ln(c_{H2})$	-
	ξ_3	7.6×10^{-5}	-
	ξ_4	-1.93×10^{-4}	-
Membrane resistivity parameter	-	12.5	-
Fuel cell capacitance	C_{dl}	0.035×232	F
Flow constant for the anode	k_a	0.065	$\text{mol s}^{-1} \text{atm}^{-1}$
Flow constant for the cathode	K_c	0.065	$\text{mol s}^{-1} \text{atm}^{-1}$
Anode volume	V_a	0.005	m^3
Cathode volume	V_c	0.01	m^3
Hydrogen enthalpy of combustion	ΔH	285.5×10^3	kJ mol^{-1}
Thermal resistance	-	0.115	C.W^{-1}
Total energy (for 6 h)	-	302.522	kWh

Table 7. Supercapacitor parameters [52].

Parameter		Value	Unit
Model	-	BCAP3000	-
Number of supercapacitors	N_{S_SC}	80	-
Rated voltage	-	2.7	V
Absolute maximum voltage	-	2.85	V
Absolute maximum current	-	1900	A
Rated capacitance	-	3000	F
Capacitance in the main cell	C_0	2100	F
-	C_1	623	F
Capacitance in the slow cell	C_2	172	F
Resistance in the main cell	R_1	0.36×10^{-3}	Ω
Resistance in the slow cell	R_2	1.92	Ω

Table 8. Battery parameters [38].

Parameter		Value	Unit
Capacity	Q_{BATmax}	6.5	Ah
Rated voltage	-	1.2	V
Battery constant voltage	E_0	1.2848	V
Internal resistance	R_{BAT}	0.0046	Ω
Number of batteries	-	360	-
Exponential zone amplitude	A_{BAT}	0.144	V
exponential zone time constant inverse	B	2.3077	$(\text{Ah})^{-1}$
Polarization resistance constant	K_{BAT}	0.01875	Ω

Regarding the working cycles in Figure 9, the characteristic line sloped down when the element moved down (i.e., the cylinder retraces and increases when the element moves up, i.e., the cylinder is extending. With the driving cycles shown in Figure 9, changes in the characteristic lines result in changes in the power required, as depicted in Figure 10, for instance, referring to the driving cycle (a) at the time of the 5th to 10th second when all three elements are moving, the power required in Figure 10

increases. Through the power curve, the power needed to run the boom was the highest compared with that of the other two; in particular, the power curve increased significantly when the boom moved up. After that, at the time of the 25th second, all elements were kept in a fixed position and the power decreased. Therefore, the buffer supplements were charged at these times as in this scenario.

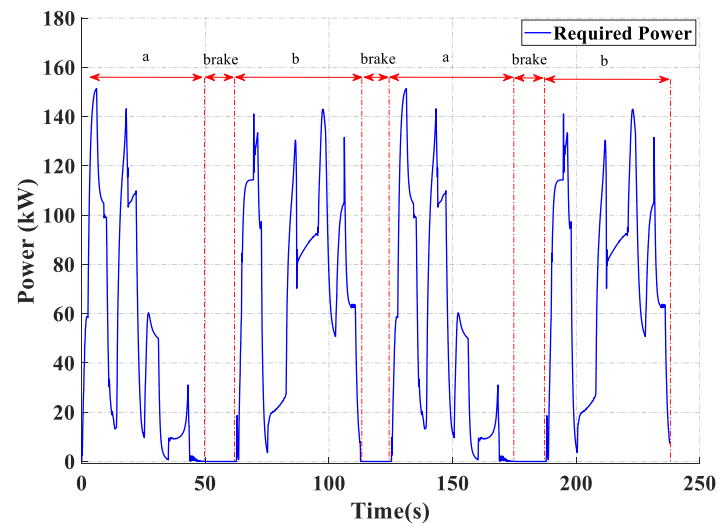


Figure 10. The required power of the excavator with two different working cycles.

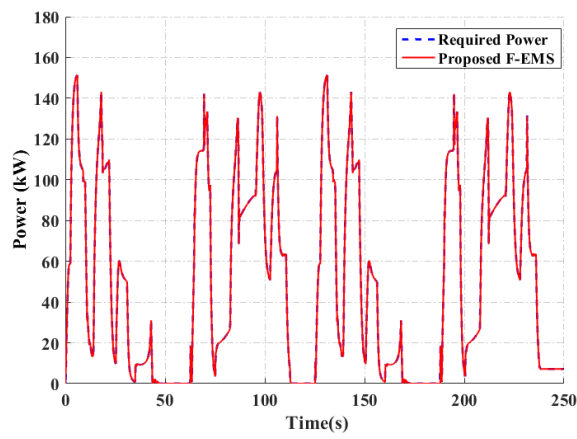
5.2. Simulation Results and Discussion

In this section, the two simulations comprising the proposed EMS in [38] and the proposed fuzzy EMS (F-EMS), as expressed in Section 3, were conducted and compared with the three other strategies: (1) conventional EMS (C-EMS) [62], (2) HFS-CS, and (3) LCS-CS in [16].

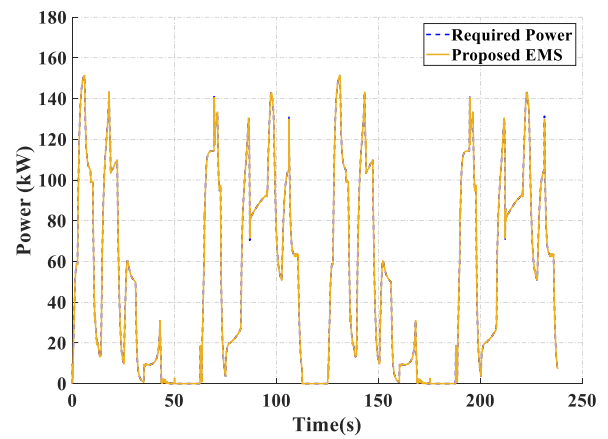
The responses of the total power supply, FC, BAT, and SC are described in Figures 11–14, respectively. In each figure, the responses when embedding the proposed EMS, proposed F-EMS, C-EMS, HFS-CS, and LCS-CS are depicted in sub-figures (a), (b), (c), (d), and (e), respectively. The total power supplied from the proposed algorithm is depicted in Figure 11a and proposed F-EMS is depicted in Figure 11b. The other results when embedding the C-EMS, HFS-CS, and LCS-CS into the system are depicted in Figure 11c–e, respectively. These results reveal that the proposed strategies can provide sufficient power to the system and maintain stable levels during an endurance process; consequently, good performance can be achieved.

In contrast, the other EMS strategies were not capable of maintaining sufficient energy. For this reason, the C-EMS did not consider the charging process for auxiliary devices when their SoC_{BAT}/SoC_{SC} dropped to a low level. When the SoC_{BAT}/SoC_{SC} reached the minimum level as shown in Figure 15, the supplements were out of power and could not support the system.

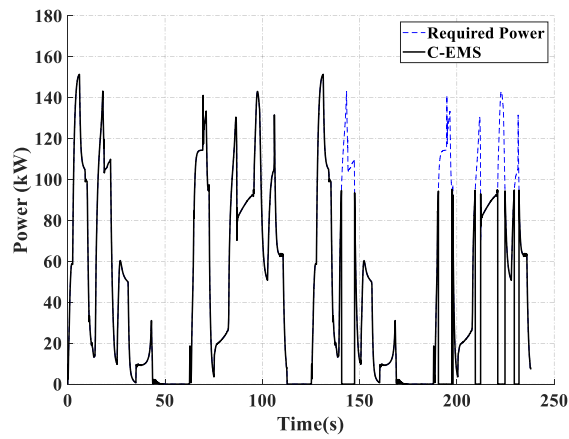
As a result, the system can not complete the requirement due to the shortage of power, starting at the time of the 140th second. For the two HFS-CS and LCS-CS strategies, charging procedures were considered in which the positive power of the auxiliary devices indicates that they are in discharge mode, whereas the negative value indicates that they are in charge mode. However, instability occurs due to the inappropriate order of using devices. Starting at the time of the 210th second, when the SoC_{BAT}/SoC_{SC} dropped down to the minimum level, the chattering phenomenon took place because the devices immediately switched from releasing to charging mode when the SoC_{BAT}/SoC_{SC} hit the minimum level. Subsequently, when the SoC_{BAT}/SoC_{SC} is greater than the minimum level, the states of the devices instantly shift from charging to releasing the power, despite low remaining power. These processes repeatedly occur and generate high-frequency fluctuations. Therefore, these paradigms need to be noticeably improved based on the fact that either the system has to stop for charging like in conventional algorithms, or employ another strategy to maintain performance.



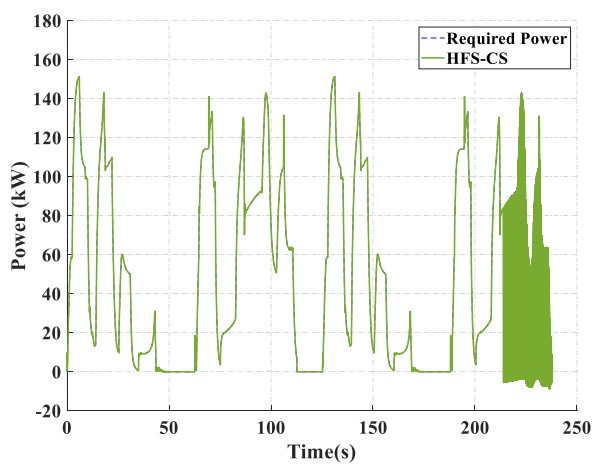
(a)



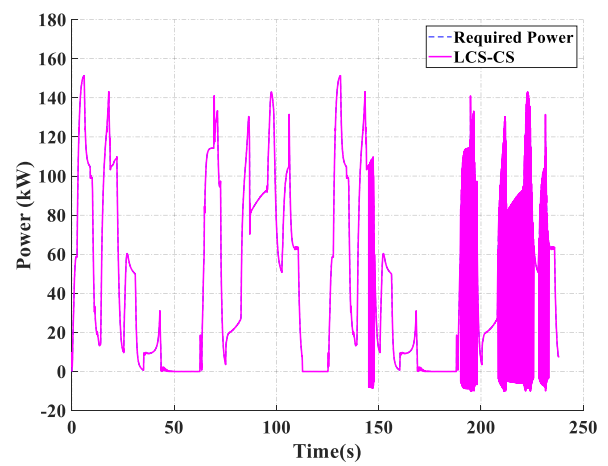
(b)



(c)



(d)



(e)

Figure 11. Power released from the HPS for the five strategies: (a) proposed F-EMS, (b) proposed EMS, (c) conventional EMS (C-EMS), (d) HFS-CS, and (e) LCS-CS.

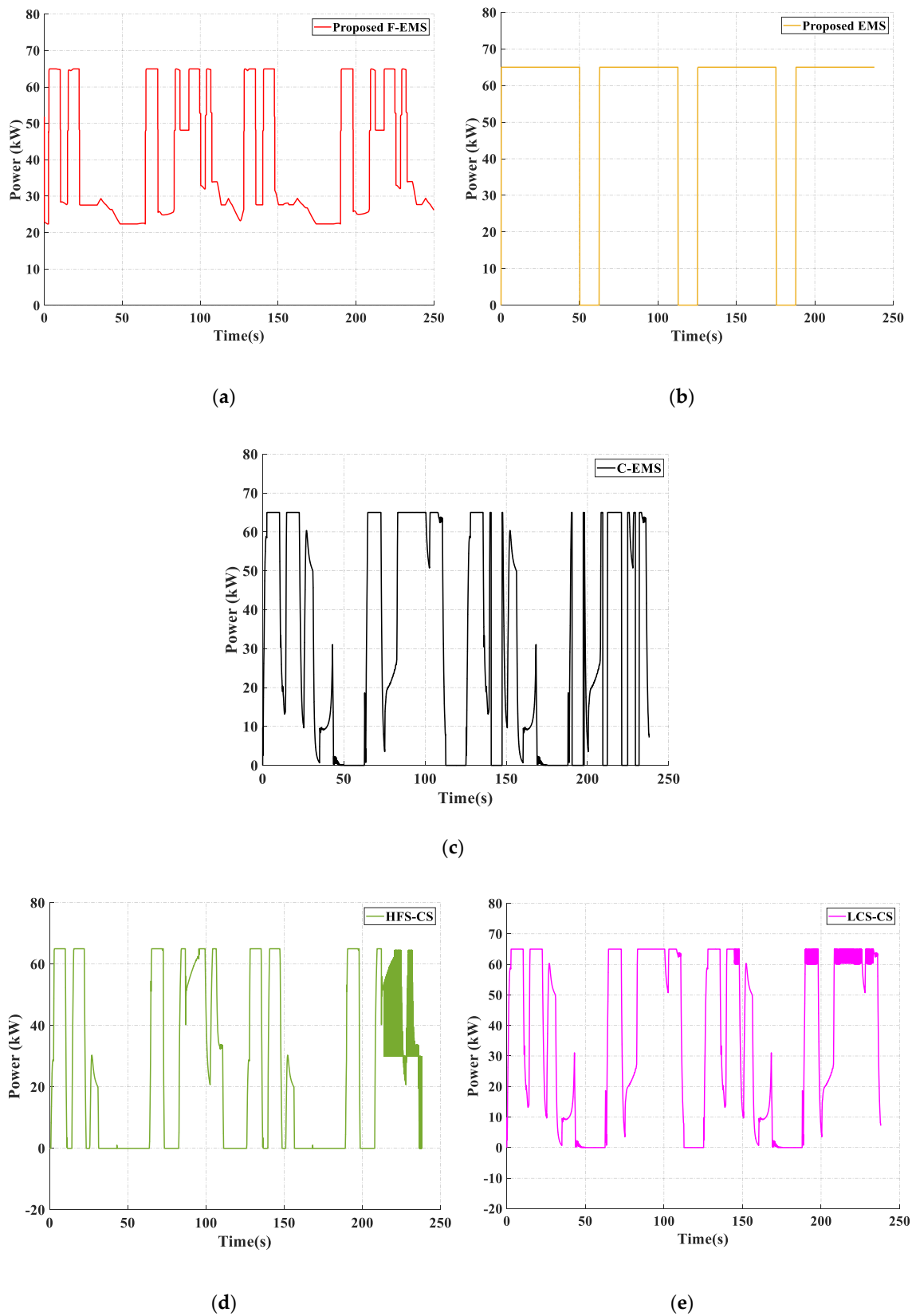


Figure 12. Power released from the FC for the five strategies: (a) proposed F-EMS, (b) proposed EMS, (c) conventional EMS (C-EMS), (d) HFS-CS, and (e) LCS-CS.

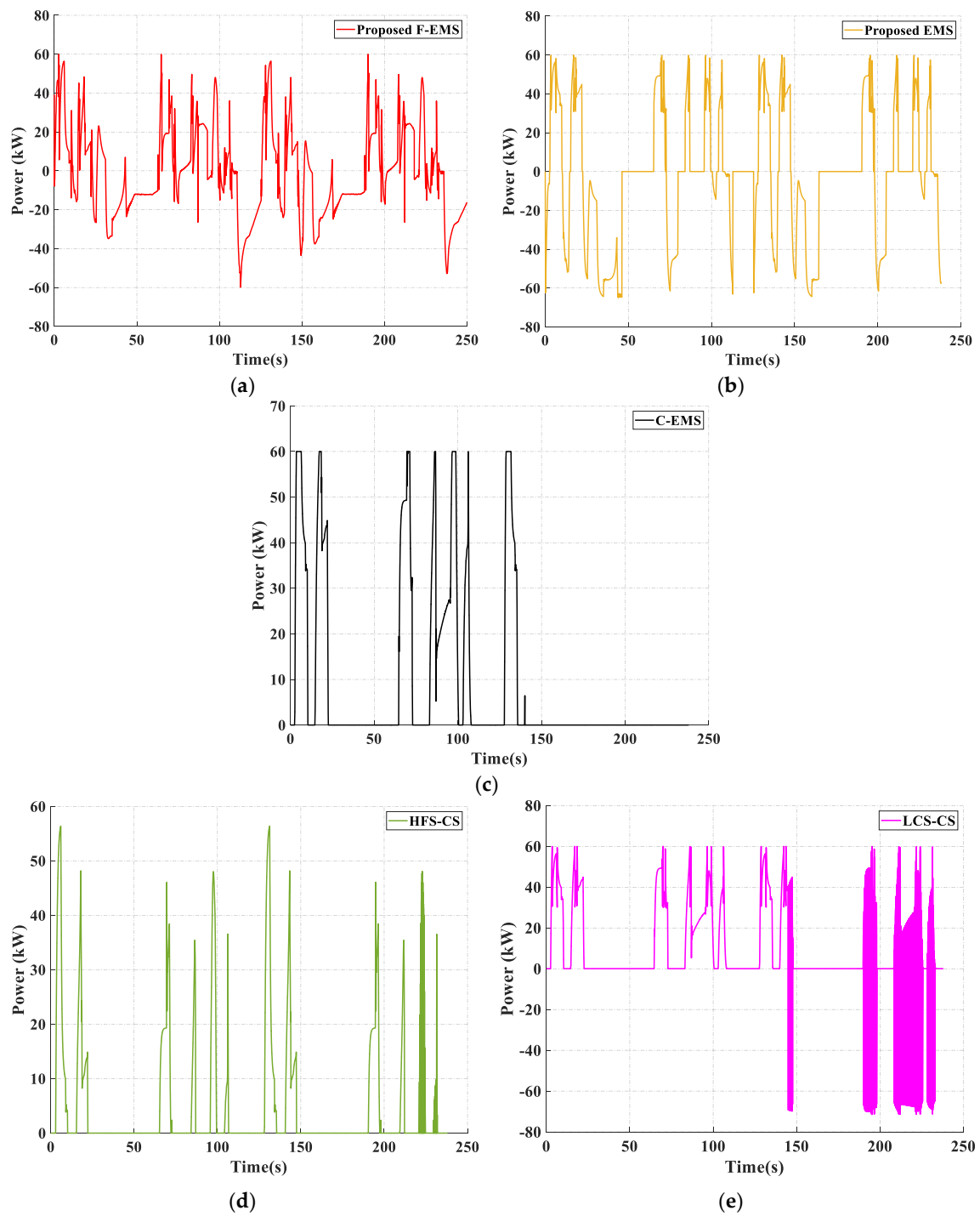
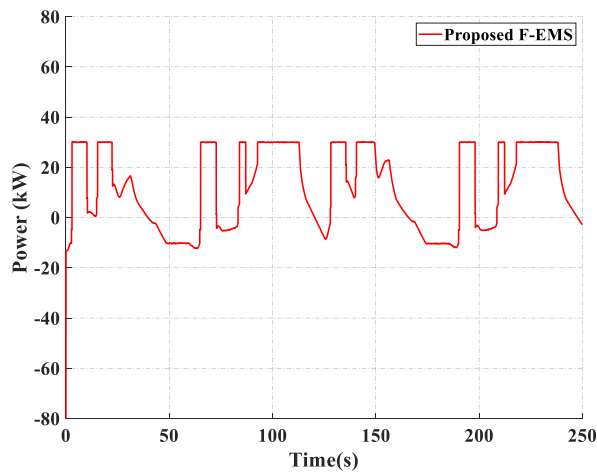
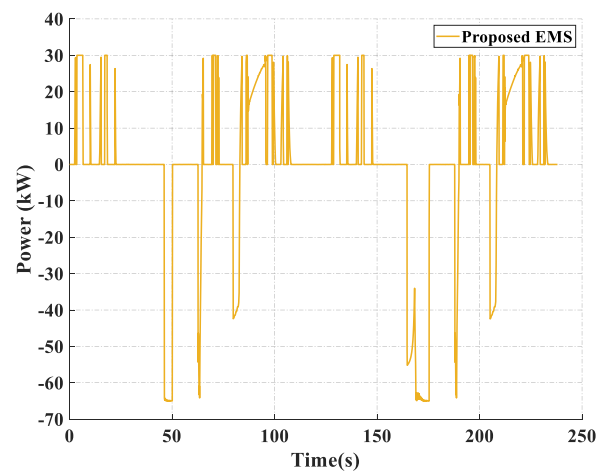


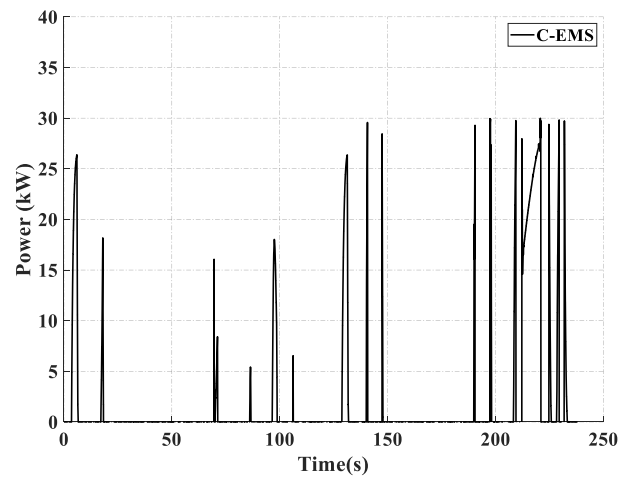
Figure 13. Power released from the SC for the five strategies: (a) proposed F-EMS, (b) proposed EMS, (c) conventional EMS (C-EMS), (d) HFS-CS, and (e) LCS-CS.



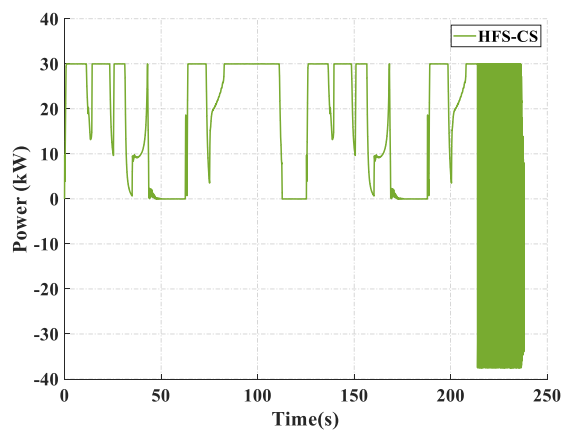
(a)



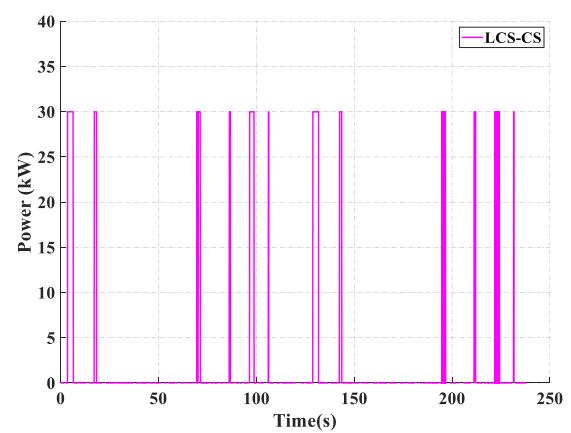
(b)



(c)



(d)



(e)

Figure 14. Power released from the BAT for the five strategies: (a) proposed F-EMS, (b) proposed EMS, (c) conventional EMS (C-EMS), (d) HFS-CS, and (e) LCS-CS.

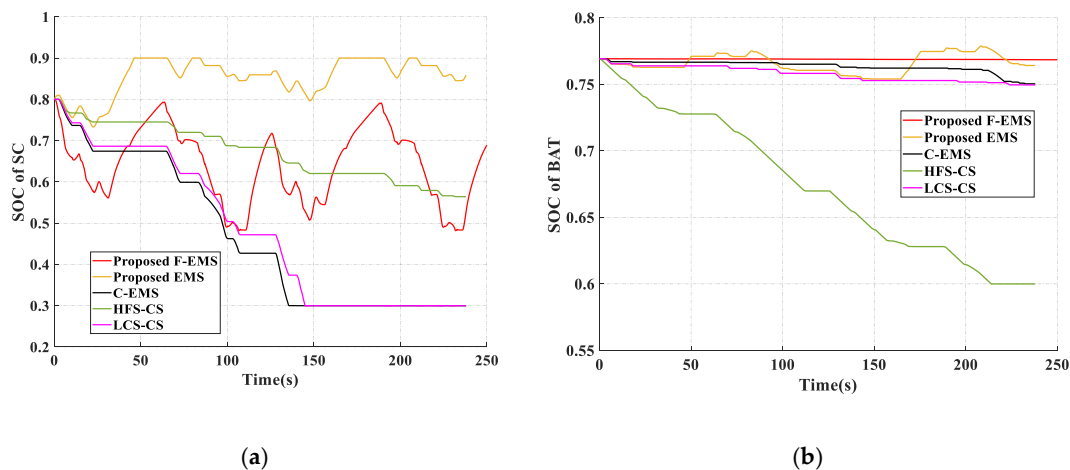


Figure 15. State of charge of (a) SC– SoC_{SC} , and (b) BAT– SoC_{BAT} .

Compared with the three previous strategies, the proposed algorithm, which considers all circumstances for stable power-sharing, has greater endurance and the supplements are considerably maintained in good condition to extend the duration for the requirements. As expressed in Figure 15, the SoC_{BAT} varied negligibly from 0.769 at the start to 0.7685 at the end of the process. The SoC_{SC} had a periodic oscillation around the value of 0.6 with a high magnitude due to the high power required. Moreover, for the proposed EMS, the P_{fc} was maintained at constant power and was only switched off in the case that no power was required. Consequently, the BAT and SC are charged every time when high power is not required. However, this is not an optimal solution for the EMS since overcharge happened in the SC at the time of the 50th second, as shown in Figure 15. Moreover, the SoC_{BAT} increased from the beginning to the end of the process because when the SC reached the maximum level, no additional power could be captured and the excess power from the FC was transferred to the BAT. Due to maintaining the constant level, the FC required more hydrogen consumption and the FC efficiency was low as a result. This issue was resolved by using the F-EMS employing the MFLC as explained in Section 4. Based on the comparison between the two proposed EMSs, the FC in the F-EMS consumes less fuel than that of the proposed EMS and is forced to the rated power to increase efficiency. The BAT takes the place of the FC in charging energy for the SC and maintaining it in good condition, instead of using the FC all the time.

Referring to the FC model in Section 2, the efficiency of the FC can be calculated as [63]

$$Eff = \frac{P_{elec}}{P_{tot}} \times \max\left(0, 1 - \frac{P_{aux}}{P_{elec}}\right) \quad (35)$$

The comparison of the efficiency for the two proposed algorithms is depicted in Figure 16.

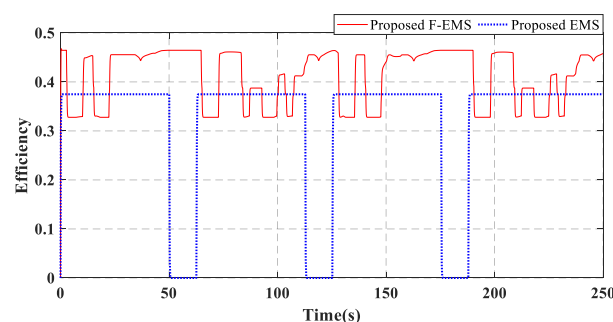


Figure 16. Efficiency comparison between the proposed EMS and proposed F-EMS.

As revealed in Figure 16, the maximum efficiency that the FC can reach when applying the proposed EMS was approximately 37% due to maintaining the constant value of 65 kW. Conversely, the efficiency when embedding the F-EMS was higher than that of the proposed EMS due to reducing the hydrogen consumption. With the response of the FC shown in Figure 12a, the efficiency of the FC could reach up to 47%. The average efficiency of the FC increased from 32% when using the proposed EMS to 42% when applying the F-EMS under the same conditions. Furthermore, the number of ON/OFF switches decreases as a solution for extending the FC lifespan.

6. Conclusions

The new configuration for the hydraulic excavators equipped with a hybrid power source comprising the fuel cell, batteries, and supercapacitors with the proposed EMS is the merit of this paper. Instead of using one auxiliary supplement until it runs out of power and using the other as a compensation supply later, the EMS was exploited to distribute the energy from the powertrain to each device so that good performance is achieved and the lifespan of all components can be extended. The simulation results displayed that the proposed EMS can satisfy the requirements in comparison with other previous approaches under different working conditions. Moreover, the generation procedure was considered as the time for healing buffer supplements. In a going effect, the use of the proposed F-EMS confirmed its effectiveness when reducing the fuel consumption in the FC while maintaining the SC in a good condition for use in the event of an emergency. The achievements in this study can not only guarantee power supply performance and prolong the lifespan of all devices, but also reduce the fuel consumption and increase the efficiency of the system. Therefore, this study is a premise for developing a hybrid power source for construction machinery in the future.

Author Contributions: K.K.A. was the supervisor providing funding and administrating the project, and he reviewed and edited the manuscript. H.V.A.T. carried out the investigation, methodology, analysis, and the validation, made the MATLAB simulation, and wrote the original manuscript. H.V.D. and T.C.D. supported to implement simulations in MATLAB and AMESim. C.M.H. carried out the illustrations and necessary figures. X.D.T. and T.D.D. checked the manuscript and supported the model for research. All authors have read and agreed to the published version of the manuscript.

Funding: This research was supported by the Basic Science Research Program through the National Research Foundation of Korea (NRF) funded by the Ministry of Science and ICT, South Korea (NRF-2020R1A2B5B03001480).

Conflicts of Interest: The authors declare no conflict of interest.

Abbreviations and Nomenclature

BAT	Batteries	p	Pump pressure
C-EMS	Conventional energy management strategy	P_{BAT}	Battery output power
EMS	Energy management strategy	p_{BPR}	Oxygen pressure at the outlet
FLS	Fuzzy logic system	p_{tank}	Pressure of the hydrogen tank
F-EMS	Fuzzy energy management strategy	P_{elec}	Electric output power
MFLC	Mapping fuzzy logic control	P_M	Motor power
HEs	Hydraulic excavators	P_p	Pump power
HPS	Hybrid power source	P_{tot}	Total power input of the system
HFS-CS	Hydrogen fuel-saving control strategy	p'_{H_2}, p'_{O_2}	Hydrogen and oxygen partial pressure
LCS-CS	Life cycle saving control strategy	Q_1, C_1	Instantaneous charge state of the supercapacitor main cell
PEMFC	Proton-exchange membrane fuel cell	Q_2, C_2	Instantaneous charge state of the supercapacitor slow cell
SC	Supercapacitors	Q_{BAT}	Instant BAT capacity
SoC_{BAT}	Battery state of charge	Q_{BATmax}	Maximum BAT capacity
SoC_{SC}	Supercapacitor state of charge	Q_{SCmax}	Maximum SC capacity
c'_{O_2}	Oxygen concentration at the cathode/membrane interface	R	Universal gas constant
		R_d	Activation resistance and concentration resistance of the FC

A	Cell area	R_{int}	Internal resistance of the electrolyte membrane
A_{BAT}	Exponential zone amplitude	R_L	Resistor of the inductor
B	Exponential zone time constant inverse	t	Time parameterized
D	Pump displacement	T	Cell temperature
E	Batteries controlled voltage source	U_{sc}	Pack supercapacitor voltage
E_{Nernst}	Voltage losses of the thermodynamic potential	v_1, v_2	Supercapacitor voltages of the first and secondary branches
F	Faraday constant	v_{sc}	Elementary SC voltage
i	Cell current	V_a	Anode volume
i_{BAT}	Battery load current and	V_{act}	Activation process voltage
i_1	Supercapacitor current through the main cell	V_{BAT}	BAT voltage
i_2	Supercapacitor current through the slow cell	V_c	Cathode volume
i_L	Currents through the inductor	V_{conc}	Concentration voltage
i_O	Output current of the converter	V_{cell}	Single cell voltage
i_{sc}	Elementary supercapacitor current	V_d	Drop voltage
I_{sc}	Pack supercapacitor current	V_{ohmic}	Ohmic voltage loss
k_a	Flow constant for the anode	V_I, V_O	DC/DC converter input and output voltage
k_c	Flow constant in cathode	V_{stack}	Fuel cell stack voltage
K_{BAT}	Polarization resistance constant	$\xi_1 \dots \xi_4$	Parametric coefficients
L	Inductance	ΔH	Hydrogen enthalpy of combustion
$\dot{m}_{H_2,in}, \dot{m}_{H_2,out}$	Hydrogen inlet and outlet flow rates through fuel cell stack	$\alpha, \beta, \gamma, \sigma$	Mapping condition coefficients
$\dot{m}_{O_2,in}, \dot{m}_{O_2,out}$	Oxygen inlet, and oxygen outlet flow rate through the fuel cell stack	η	Pump volumetric efficiency
n	Pump rotational speed	η_{DC}	The converter efficient
N	Number of cells	η_M	Efficiency of converting electric power to mechanical power
N_{s_sc}	Number of supercapacitors in serial connection	κ_{DC}	Ratio of the DC/DC converter output and input voltage
N_{p_sc}	Number of supercapacitors in parallel branches		

References

- Oh, K.S.; Seo, J.H. Inertial Parameter Estimation of an Excavator with Adaptive Updating Rule Using Performance Analysis of Kalman Filter. *Int. J. Control Autom. Syst.* **2018**, *16*, 1226–1238. [[CrossRef](#)]
- Kim, S.H.; Park, J.M.; Kang, S.H.; Kim, P.Y.; Kim, H.J. A Robust Control Approach for Hydraulic Excavators Using μ -synthesis. *Int. J. Control Autom. Syst.* **2018**, *16*, 1615–1628. [[CrossRef](#)]
- Park, H.G.; Nahian, S.A.; Ahn, K.K. A Study on Energy Saving of IMV Circuit Using Pressure Feedback. *J. Drive Control* **2016**, *13*, 31–44. [[CrossRef](#)]
- Sun, H.; Yang, L.F.; Jing, J.Q.; Luo, Y.L. Control strategy of hydraulic/electric synergy system in heavy hybrid vehicles. *Energy Convers. Manag.* **2011**, *52*, 668–674.
- Ahn, K.K.; Ho, T.H.; Dinh, Q.T. A study on energy saving potential of hydraulic control system using switching type closed loop constant pressure system. In Proceedings of the JFPS International Symposium on Fluid Power, TOYAMA 2008, Toyama, Japan, 15–18 September 2008; pp. 317–322.
- Ahn, K.K.; Dinh, Q.T. Development of energy saving hybrid excavator using hybrid actuator. In Proceedings of the 7th International Conference on Fluid Power Transmission and Control 2009, Hangzhou, China, 7–10 April 2009; pp. 205–209.
- Ho, T.H.; Ahn, K.K. Saving energy control of cylinder drive using hydraulic transformer combined with an assisted hydraulic circuit. In Proceedings of the ICROS-SICE International Joint Conference 2009, Fukuoka, Japan, 18–21 August 2009; pp. 2115–2120.

8. Ahn, K.K.; Ji, Y. Development of Hybrid Excavator for Regeneration of Boom Potential Energy. *J. Drive Control* **2010**, *7*, 25–32.
9. Jeong, E.J.; Seo, B.M.; Ahn, K.K. A Trend of Electro-Hydraulic System Technology for Construction Equipment. *J. Drive Control* **2018**, *15*, 73–79.
10. Yu, Y.X.; Jeong, E.J.; Ahn, K.K. Review of Energy Saving Technology of Hybrid Construction Machine. *J. Drive Control* **2018**, *15*, 91–100.
11. Shen, W.; Jiang, J.H.; Su, X.Y.; Karimi, H.R. Parameter Matching Analysis of Hydraulic Hybrid Excavators Based on Dynamic Programming Algorithm. *J. Appl. Math.* **2013**, *2013*, 1–10. [[CrossRef](#)]
12. Yi, H.S.; Jeong, J.B.; Cha, S.W.; Zheng, C.H. Optimal Component Sizing of Fuel Cell-Battery Excavator Based on Workload. *IJPEM-GT* **2018**, *5*, 103–110. [[CrossRef](#)]
13. Gong, J.; He, Q.H.; Zhang, D.; Zhang, Y.L.; Liu, X.H. Power System Control Strategy for Hybrid Excavator Based on Equivalent Fuel Consumption. In Proceedings of the 2012 IEEE International Conference on Mechatronics and Automation, Chengdu, China, 5–8 August 2012.
14. Li, T.; Liu, H.; Zhao, D.X.; Wang, L. Design and analysis of a fuel cell supercapacitor hybrid construction vehicle. *Int. J. Hydrogen Energy* **2016**, *41*, 12307–12319. [[CrossRef](#)]
15. Li, T.; Liu, H.; Ding, D. Predictive energy management of fuel cell supercapacitor hybrid construction equipment. *Energy* **2018**, *149*, 718–729. [[CrossRef](#)]
16. Li, T.; Huang, L.; Liu, H. Energy management and economic analysis for a fuel cell supercapacitor excavator. *Energy* **2019**, *172*, 840–851. [[CrossRef](#)]
17. Zhang, Y.; Li, Y.W. Energy Management Strategy for Supercapacitor in Droop-Controlled DC Microgrid Using Virtual Impedance. *IEEE Trans. Power Electron.* **2017**, *32*, 2704–2716. [[CrossRef](#)]
18. Vanessa, P.; Donato, T.; Risi, A.D.; Laforgia, D. Super-capacitors fuel-cell hybrid electric vehicle optimization and control strategy development. *Energy Convers. Manag.* **2007**, *48*, 3001–3008.
19. Kaya, K.; Hames, Y. Two new control strategies: For hydrogen fuel saving and extend the life cycle in the hydrogen fuel cell vehicles. *Int. J. Hydrogen Energy* **2019**, *44*, 18967–18980. [[CrossRef](#)]
20. Zhang, W.B.; Li, J.Q.; Xu, L.F.; Minggao, O. Optimization for a fuel cell/battery/capacity tram with equivalent consumption minimization strategy. *Energy Convers. Manag.* **2017**, *134*, 59–69. [[CrossRef](#)]
21. Salahuddin, U.; Ejaz, H.; Iqbal, N. Grid to wheel energy efficiency analysis of battery-and fuel cell-powered vehicles. *Int. J. Energy Res.* **2018**, *42*, 2021–2028. [[CrossRef](#)]
22. Fletcher, T.; Thringer, R.; Watkinson, M. An Energy Management Strategy to concurrently optimise fuel consumption & PEM fuel cell lifetime in a hybrid vehicle. *Int. J. Hydrogen Energy* **2016**, *41*, 21503–21515.
23. Kasimalla, V.K.R.; Naga, S.G.; Velisala, V. A review on energy allocation of fuelcell/battery/ultracapacitor for hybrid electric vehicles. *Int. J. Energy Res.* **2018**, *42*, 4263–4283. [[CrossRef](#)]
24. Melero-Perez, A.; Gao, W.Z.; Fernández-Lozano, J. Fuzzy Logic Energy Management Strategy for Fuel Cell/Ultracapacitor/Battery Hybrid Vehicle with Multiple-Input DC/DC Converter. In Proceedings of the IEEE Vehicle Power and Propulsion Conference, Dearborn, MI, USA, 7–10 September 2009; pp. 199–206.
25. Li, S.G.; Sharkh, S.M.; Walsh, F.C.; Zhang, C.N. Energy and Battery Management of a Plug-In Series Hybrid Electric Vehicle Using Fuzzy Logic. *IEEE Trans. Veh. Technol.* **2011**, *60*, 3571–3585. [[CrossRef](#)]
26. Li, Q.; Chen, W.R.; Li, Y.K.; Liu, S.K.; Huang, J. Energy management strategy for fuel cell/battery/ultracapacitor hybrid vehicle based on fuzzy logic. *Electr. Power Energy Syst.* **2012**, *43*, 514–525. [[CrossRef](#)]
27. Abadlia, I.; Bahi, T.; Bouzeria, H. Energy management strategy based on fuzzy logic for compound RES/ESS used in stand-alone application. *Int. J. Hydrogen Energy* **2016**, *41*, 16705–16717. [[CrossRef](#)]
28. Peng, F.; Zhao, Y.Z.; Li, X.P.; Liu, Z.X.; Chen, W.R.; Liu, Y.; Zhou, D.H. Development of master-slave energy management strategy based on fuzzy logic hysteresis state machine and differential power processing compensation for a PEMFC-LIB-SC hybrid tramway. *Appl. Energy* **2017**, *206*, 346–363. [[CrossRef](#)]
29. Ahmadi, S.; Bathaee, S.M.T.; Hosseinpour, A.H. Improving fuel economy and performance of a fuel-cell hybrid electric vehicle (fuel-cell, battery, and ultra-capacitor) using optimized energy management strategy. *Energy Convers. Manag.* **2018**, *160*, 74–84. [[CrossRef](#)]
30. Hames, Y.; Kaya, K.; Baltacioglu, E.; Turksoy, A. Analysis of the control strategies for fuel saving in the hydrogen fuel cell vehicles. *Int. J. Hydrogen Energy* **2018**, *43*, 10810–10821. [[CrossRef](#)]
31. Zhang, X.H.; Liu, L.; Dai, Y.L.; Lu, T.H. Experimental investigation on the online fuzzy energy management of hybrid fuel cell/battery power system for UAVs. *Int. J. Hydrogen Energy* **2018**, *43*, 10094–10103. [[CrossRef](#)]

32. Geng, C.; Jin, X.F.; Zhang, X. Simulation research on a novel control strategy for fuel cell extended-range vehicles. *Int. J. Hydrogen Energy* **2019**, *44*, 408–420. [[CrossRef](#)]
33. Eckert, J.J.; Silva, L.C.A.; Santicioli, F.M.; Costa, E.D.; Corrêa, F.C.; Dedini, F.G. Energy storage and control optimization for an electric vehicle. *Int. J. Energy Res.* **2018**, *42*, 3506–3523. [[CrossRef](#)]
34. Ameer, K.; Hadjaissa, A.; Ait-Cheikh, M.S.; Chekneane, A.; Essounbouli, N. Fuzzy energy management of hybrid renewable power system with the aim to extend component lifetime. *Int. J. Energy Res.* **2017**, *41*, 1867–1879. [[CrossRef](#)]
35. Do, H.T.; Ahn, K.K. Velocity control of a secondary controlled closed-loop hydrostatic transmission system using an adaptive fuzzy sliding mode controller. *J. Mech. Sci. Technol.* **2013**, *27*, 875–884. [[CrossRef](#)]
36. Dao, T.L.; Dinh, Q.T.; Ahn, K.K. A torque estimator using online tuning grey fuzzy PID for applications to torque-sensorless control of DC motors. *Mechatronics* **2015**, *26*, 45–63.
37. Le, D.H.; Ahn, K.K.; Nguyen, B.K.; Jo, W.K. Trajectory control of electro-hydraulic excavator using fuzzy self-tuning algorithm with neural network. *J. Mech. Sci. Technol.* **2009**, *23*, 149–160.
38. Do, T.C.; Truong, H.V.A.; Dao, H.V.; Ho, C.M.; To, X.D.; Dang, T.D.; Ahn, K.K. Energy management strategy of a PEM fuel cell excavator with supercapacitor/battery hybrid power source. *Energies* **2019**, *12*, 4362. [[CrossRef](#)]
39. Pinches, M.J.; Ashby, J.G. *Power Hydraulic*; Prentice Hall Inc.: Englewood Cliffs, NJ, USA, 1988.
40. Siemens LMS AMESim AME Sim Help: Example. Available online: <https://www.plm.automation.siemens.com/global/en/search.html?query=help&lang=en> (accessed on 5 March 2020).
41. Khan, M.J.; Iqbal, M.T. Modelling and Analysis of Electro-chemical, Thermal, and Reactant Flow Dynamics for a PEM Fuel Cell System. *Fuel Cells* **2005**, *5*, 463–475. [[CrossRef](#)]
42. Sankar, K.; Aguan, K.; Jana, A.K. A proton exchange membrane fuel cell with an airflow cooling system: Dynamics, validation and nonlinear control. *Energy Convers. Manag.* **2019**, *183*, 230–240. [[CrossRef](#)]
43. Musio, F.; Tacchi, F.; Omati, L.; Stampino, P.G.; Dotelli, G.; Limonta, S.; Brivio, D.; Grassini, P. PEMFC system simulation in MATLAB-Simulink® environment. *Int. J. Hydrogen Energy* **2011**, *36*, 8045–8052. [[CrossRef](#)]
44. Dang, T.D.; Do, T.C.; Truong, H.V.A.; Ho, C.M.; Dao, H.V.; Yu, Y.X.; Jeong, E.J.; Ahn, K.K. Design, Modeling and Analysis of a PEM Fuel Cell Excavator with Supercapacitor/Battery Hybrid Power Source. *J. Drive Control* **2019**, *16*, 45–53.
45. Pukrushpan, J.T. Modeling and Control of Fuel Cell Systems and Fuel Processor. Ph.D. Thesis, Department of Mechanical Engineering, The University of Michigan, Ann Arbor, MI, USA, 2003.
46. Erdinc, O.; Vural, B.; Uzunoglu, B. A wavelet-fuzzy logic based energy management strategy for a fuel cell/battery/ultra-capacitor hybrid vehicular power system. *J. Power Sources* **2009**, *194*, 369–380. [[CrossRef](#)]
47. Uzunoglu, M.; Alam, M.S. Dynamic modeling, design and simulation of a PEM fuel cell/ultra-capacitor hybrid system for vehicular applications. *Energy Convers. Manag.* **2007**, *48*, 1544–1553. [[CrossRef](#)]
48. Thounthong, P.; Rael, S.; Davat, B. Analysis of Supercapacitor as Second Source Based on Fuel Cell Power Generation. *IEEE Trans. Energy Convers.* **2009**, *24*, 247–255. [[CrossRef](#)]
49. Lei, Z.G.; Huc, X.S.; Zhenpo, W.; Suna, F.C.; David, G.D. A review of supercapacitor modeling, estimation, and applications: A control/management perspective. *Renew. Sustain. Energy Rev.* **2018**, *81*, 1868–1878.
50. Zubieta, L.; Bonert, R. Characterization of Double-Layer Capacitors for Power Electronics Applications. *IEEE Trans. Ind. Appl.* **2000**, *36*, 199–205. [[CrossRef](#)]
51. Pagano, M.; Piegari, L. Hybrid electrochemical power sources for onboard applications. *IEEE Trans. Energy Convers.* **2007**, *22*, 450–456. [[CrossRef](#)]
52. Lahyani, A.; Venet, P.; Guermazi, A.; Troudi, A. Battery/Supercapacitors Combination in Uninterruptible Power Supply (UPS). *IEEE Trans. Power Electron.* **2013**, *28*, 1509–1522. [[CrossRef](#)]
53. Gualous, H.; Bouquain, D.; Berthon, A.; Kauffmann, J.M. Experimental study of supercapacitor serial resistance and capacitance variations with temperature. *J. Power Sources* **2003**, *123*, 86–93. [[CrossRef](#)]
54. Saha, P.; Khanra, M. Equivalent Circuit Model of Supercapacitor for Self-Discharge Analysis—A Comparative Study. In Proceedings of the International conference on Signal Processing, Communication, Power and Embedded System (SCOPEs), Odisha, India, 3–5 October 2016; pp. 1381–1386.
55. Benyahia, N.; Denoun, H.; Zaouia, M.; Tamalouzt, S.; Bouheraoua, M.; Benamrouche, N.; Rekioua, T.; Haddad, S. Characterization and Control of Supercapacitors Bank for Stand-Alone Photovoltaic Energy. *Energy Procedia* **2013**, *42*, 539–548. [[CrossRef](#)]

56. Tremblay, O.; Dessaint, L.A. Experimental validation of a battery dynamic model for EV applications. *World Electr. Veh. J.* **2009**, *3*, 289–298. [[CrossRef](#)]
57. Hannan, M.A.; Azidin, F.A.; Mohamed, A. Multi-sources model and control algorithm of an energy management system for light electric vehicles. *Energy Convers. Manag.* **2012**, *62*, 123–130. [[CrossRef](#)]
58. Fernandez, L.M.; Garcia, P.; Garcia, C.A.; Jurado, F. Hybrid electric system based on fuel cell and battery and integrating a single dc/dc converter for a tramway. *Energy Convers. Manag.* **2011**, *52*, 2183–2192. [[CrossRef](#)]
59. Castaings, A.; Lhomme, W.; Trigui, R.; Bouscayrol, A. Practical control schemes of a battery/supercapacitor system for electric vehicle. *IET Electr. Syst. Transp.* **2016**, *6*, 20–26. [[CrossRef](#)]
60. To, X.D.; Le, K.T.; Nguyen, T.T.; Dang, T.D.; Ho, C.M.; Truong, H.V.A.; Dao, H.V.; Do, T.C.; Ahn, K.K. Modeling and Energy Management Strategy in Energetic Macroscopic Representation for a Fuel Cell Hybrid Electric Vehicle. *J. Drive Control* **2019**, *16*, 80–90.
61. Nguyen, B.; German, R.; Trovão, J.P.F.; Bouscayrol, A. Real-Time Energy Management of Battery/Supercapacitor Electric Vehicles Based on an Adaptation of Pontryagin’s Minimum Principle. *IEEE Trans. Veh. Technol.* **2019**, *68*, 203–212. [[CrossRef](#)]
62. Fathabadi, H. Novel fuel cell/battery/supercapacitor hybrid power source for fuel cell hybrid electric vehicles. *Energy* **2018**, *143*, 467–477. [[CrossRef](#)]
63. Trevor, H.K.; Wu, X.F.; Yao, Q.H. Multi-objective genetic optimization of the thermoelectric system for thermal management of proton exchange membrane fuel cells. *Appl. Energy* **2018**, *217*, 214–327.



© 2020 by the authors. Licensee MDPI, Basel, Switzerland. This article is an open access article distributed under the terms and conditions of the Creative Commons Attribution (CC BY) license (<http://creativecommons.org/licenses/by/4.0/>).